Journal of the Korean Physical Society, Vol. 54, No. 4, April 2009, pp. 1685∼1691

Impact of Polarization Inside a Resist for ArF Immersion Lithography

Sang-Kon Kim,* Hye-Keun Oh, Young-Dae Jung and Ilsin An
Department of Applied Physics, Hanyang University, Ansan 426-791

(Received 31 March 2008, in final form 14 January 2009)

Immersion technology with new lens materials and new high-refractive fluids is the key technology to extend the resolution capability of existing 193-nm lithography below the 32-nm pattern formation, but it faces more pronounced polarization and reflection control issues. In this paper, for a wet system, the propagations of the transverse electric (TE) and the transverse magnetic (TM) waves inside a one-layer resist and a multi-layer resist are described by using the finite-difference-time-domain (FDTD) method with a multi-layer model and a transfer-matrix model, respectively. In the comparison with a dry system, the TE and the TM modes of the wet system are larger than those of the dry system. Inside the multi-layer resist, the TM and the TE modes change little at incident angle below 20°. However, for a 45-nm pattern formation, no difference between the TM and the TE modes is found under the given conditions for incident angles below 20°.

PACS numbers: 85.40.HP, 78.20.Bh, 85.40.Bh
Keywords: Lithography, Lithography simulation, Immersion lithography, Finite-difference time domain, Polarization

I. INTRODUCTION

F_2 (157-nm) lithography development faces several crucial issues, such as CaF_2 birefringence, resists and pellicles. Also, the substitute of a new wavelength (extreme ultraviolet (EUV)) tool takes more time than expected and the estimated high cost is becoming a great concern. Immersion lithography has been proposed as a method of improving the resolution of optical lithography and is rapidly emerging as an important candidate for upcoming semiconductor lithography applications because immersion lithography can be readily applied to extend optical lithography without significant changes to the infrastructure that has been used for decades. Immersion lithography is a technology in which a liquid with a high refractive index is filled between the lens and the resist. As the refractive index of water is 1.43664, the numerical aperture (NA) is $1.43664 \times \sin\theta$. Due to the Rayleigh of the half-pitch size of a pattern (=$k_1\cdot$ wavelength/NA), the half pitch can be 33.6 nm (=0.25 · 193/1.43664) for $k_1 = 0.25$, NA = 1.43664 and wavelength = 193 nm [1].

In order to understand immersion lithography with high and hyper NA, vector effects and polarization characteristics have been researched. Polarization effects of high NA in the mask and the optical lithography system are modeled to solve problems by applying the optical system design and the lithography processes for a fine pattern formation [2–4]. However, wave propagation through thin films can cause polarization-dependent behavior due to angle of incidence and polarization inside the resist depends on the change in the resists refractive index and in the absorption due to the photoactive chemical amplitude. Although the incident light propagates normally into the resist, the light can propagate with a non-normal angle inside a multi-layer resist and the light can be reflected with a non-normal angle from an anti-reflective coating (ARC) because the distribution of resist molecules is not uniform.

In this paper, immersion effects are described by using analytical approaches. For a one-layer resist, the wave propagation of the transverse electric (TE) and the transverse magnetic (TM) modes inside resist is simulated by using the finite-difference-time-domain (FDTD) method. For a multi-layer resist, aerial images of the TM and the TE modes due to incident angles are described by using a multi-layer model and a transfer-matrix model.

II. EFFECTS OF IMMERSION LIQUID

The propagation of electromagnetic waves in a dielectric medium corresponds to the time-dependent Maxell's curl equations:

$$\nabla \cdot \vec{D} = \nabla \cdot \left(\varepsilon \vec{E}\right) = 0, \nabla \times \vec{E} = -\frac{\partial \vec{B}}{\partial t} = -\mu_0 \frac{\partial \vec{H}}{\partial t}, \quad (1)$$

*E-mail: sangkona@hotmail.com; http://www.sangkon.info

$$\nabla \cdot \vec{H} = 0, \nabla \times \vec{H} = \vec{j} + \frac{\partial \vec{D}}{\partial t} = \sigma \vec{E} + \varepsilon \frac{\partial \vec{E}}{\partial t}, \tag{2}$$

where $\vec{E}\left(\vec{B}\right)$ is the electric (magnetic) field, $\vec{H}$ is the magnetic intensity, $\vec{D}$ is the electric displacement, $\vec{J}$ is the current density, μ_0 is the permeability, $\varepsilon\,(=\varepsilon_r\varepsilon_0)$ is the permittivity and σ is the conductivity. When conductivity is zero, Eqs. (1) and (2) are

$$\frac{\partial \tilde{E}}{\partial t} = \frac{1}{\varepsilon_r \varepsilon_0} \nabla \times \vec{H}, \frac{\partial \vec{H}}{\partial t} = -\frac{1}{\mu_0} \nabla \times \vec{E},$$
$$\vec{D}(w) = \varepsilon_r^*(\omega) \cdot \tilde{E}(w). \tag{3}$$

In one-dimension, Maxwell's equations in Eq. (3) can be rewritten as

$$\frac{\partial \tilde{E}_x(t)}{\partial t} = \frac{1}{\varepsilon_r \sqrt{\varepsilon_0 \mu_0}} \frac{\partial H_y(t)}{\partial z},$$
$$\frac{\partial H_y(t)}{\partial t} = -\frac{1}{\sqrt{\varepsilon_0 \mu_0}} \frac{\partial \tilde{E}_x(t)}{\partial z}. \tag{4}$$

Hence, the electromagnetic waves in FDTD notation are

$$\frac{\tilde{E}_x^{\;n+1/2}(k) - \tilde{E}_x^{\;n-1/2}(k)}{\Delta t} = \frac{1}{\varepsilon_r \sqrt{\varepsilon_0 \mu_0}} \frac{H_y^n(k+1/2) - H_y^n(k+1/2)}{\Delta x}, \tag{5}$$

$$\frac{H_y^{n+1}(k+1/2) - H_y^n(k+1/2)}{\Delta t} = -\frac{1}{\mu_0} \frac{\tilde{E}_x^{\;n+1/2}(k+1) - \tilde{E}_x^{\;n+1/2}(k)}{\Delta x}, \tag{6}$$

In two-dimension, the FDTD equations (H_x, H_y, E_z) of the TM mode are

$$\frac{D_z^{n+1/2}(i,j) - D_z^{n-1/2}(i,j)}{\Delta t} = \frac{1}{\sqrt{\varepsilon_0 \mu_0}} \left(\frac{H_y^n(i+1/2,j) - H_y^n(i-1/2,j)}{\Delta x} \right) - \frac{1}{\sqrt{\varepsilon_0 \mu_0}} \left(\frac{H_x^n(i,j+1/2) - H_x^n(i,j-1/2)}{\Delta x} \right), \tag{7}$$

$$\frac{H_x^{n+1}(i,j+1/2) - H_x^n(i,j-1/2)}{\Delta t} = -\frac{1}{\sqrt{\varepsilon_0 \mu_0}} \frac{E_z^{n+1/2}(i,j+1) - E_z^{n+1/2}(i,j)}{\Delta x}, \tag{8}$$

$$\frac{H_y^{n+1}(i+1/2,j) - H_y^n(i+1/2,j)}{\Delta t} = \frac{1}{\sqrt{\varepsilon_0 \mu_0}} \frac{E_z^{n+1/2}(i+1,j) - E_z^{n+1/2}(i,j)}{\Delta x}, \tag{9}$$

and the FDTD equations (E_x, E_y, H_z) of the TE mode are

$$\frac{H_z^{n+1/2}(i,j) - H_z^{n-1/2}(i,j)}{\Delta t} = -\frac{1}{\sqrt{\varepsilon_0 \mu_0}} \left(\frac{E_y^n(i+1/2,j) - E_y^n(i-1/2,j)}{\Delta x} \right) + \frac{1}{\sqrt{\varepsilon_0 \mu_0}} \left(\frac{E_x^n(i,j+1/2) - E_x^n(i,j-1/2)}{\Delta x} \right), \tag{10}$$

$$\frac{D_x^{n+1}(i,j+1/2) - D_x^n(i,j-1/2)}{\Delta t} = \frac{1}{\sqrt{\varepsilon_0 \mu_0}} \frac{H_z^{n+1/2}(i,j+1) - H_z^{n+12}(i,j)}{\Delta x}, \tag{11}$$

$$\frac{D_y^{n+1}(i+1/2,j) - D_y^n(i+1/2,j)}{\Delta t} = -\frac{1}{\sqrt{\varepsilon_0 \mu_0}} \frac{H_z^{n+1/2}(i+1,j) - H_z^{n+1/2}(i,j)}{\Delta x}, \tag{12}$$

Figure 1 shows the one-dimensional propagation of electric fields (E_x) and magnetic fields (H_y) in a dry system and a wet system, which were obtained by Eqs. (5) and (6). The dry system is an air (ε_1) / resist (ε_3) system in Figures 1(a1)-(b4) and the wet system is an air (ε_1) / water (ε_2) / resist (ε_3) system in Figures 1(c1)-(d4). For both systems, it is hard to compare the transmittances of the electric field and the magnetic field due to the permittivity of resist. However, the reflection in the dry system at circle A in Figure 1(a4) is larger than that of the wet system at circle B in Figure 1(c4).

Figure 2 shows the two-dimensional propagation of the electric fields (E_z) in the TM mode (H_x, H_y, E_z), which were obtained by using Eqs. (7)-(9). Figures 2(b) and (c) are simulated results for the wet system (air (ε_1) / water (ε_2) / resist (ε_3)) and Figures 2(d) and (e) are simulated results for the dry system (air (ε_1) / resist (ε_3)). Although it is hard to compare the two-dimensional results, the reflection in the wet system is smaller than that in the dry system according to the one-dimensional results of Figure 2(f). The peak of circle A in Figure 2(c) is produced due to boundary conditions.

Figure 3 shows the two-dimensional propagation of the magnetic fields (H_z) in the TE mode (E_x, E_y, H_z) which were obtained by using Eqs. (10)-(12). In comparison with reflection in the dry system in Figure 3(e), the reflection in the wet system in Figures 3(c) and (f) is smaller. It is the same immersion effects as for the electric field (E_z) of Figure 2.

Simulation results of Figures 1-3 are based on a one-layer resist, for which wave magnitude is assumed not to be reduced due to the thickness of one layer. In both the one-dimensional results in Figure 1 and the two-dimensional results in Figures 2 and 3, the reflection in the wet system is smaller than that in the dry system at the resist surface. The transmittance of the wet system is expected to be larger than that of the dry system. In comparison with the intensity of the TM expected to be peak in Figure 2(f), the intensity of the TE peak in Figure 3(f) is larger. The TE mode is expected to be larger than the TM mode inside the resist.

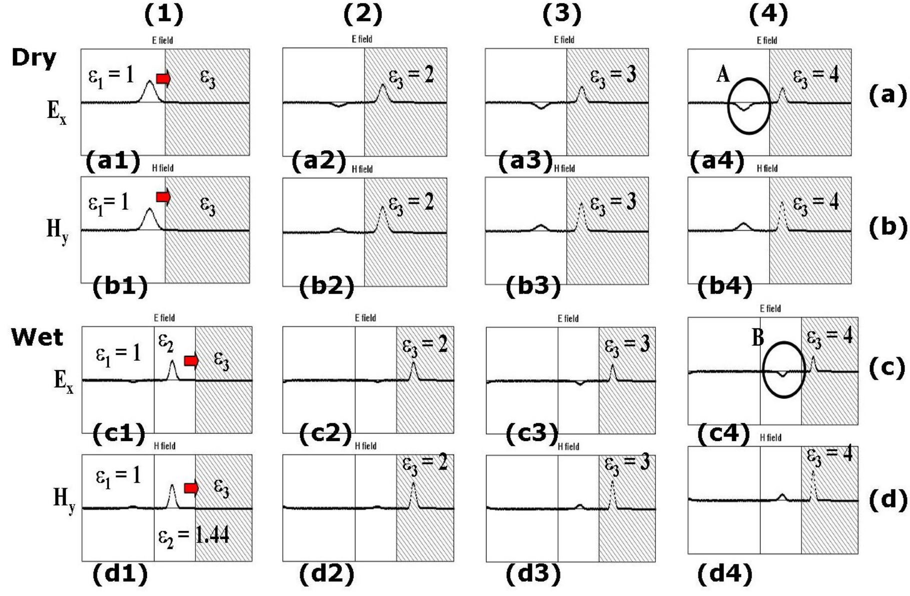

Fig. 1. One-dimensional propagation of (a) electric fields (E_x) and (b) magnetic fields (H_y) into a dry system (air ($\varepsilon_1 = 1$) / resist (ε_3)), (c) electric fields and (d) magnetic fields into a wet system (air ($\varepsilon_1 = 1$) / water ($\varepsilon_2 = 1.446$) / resist (ε_3)) by using Eqs. (5) and (6): (1) incident waves in air and (2)-(3) transmitted waves due to the permittivity ($\varepsilon_1 = 2$, 3 and 4, respectively) of the resist. The circle A in Figure 1 (a4) and circle B in Figure 1 (c4) are reflected waves for the dry system and the wet system, respectively.

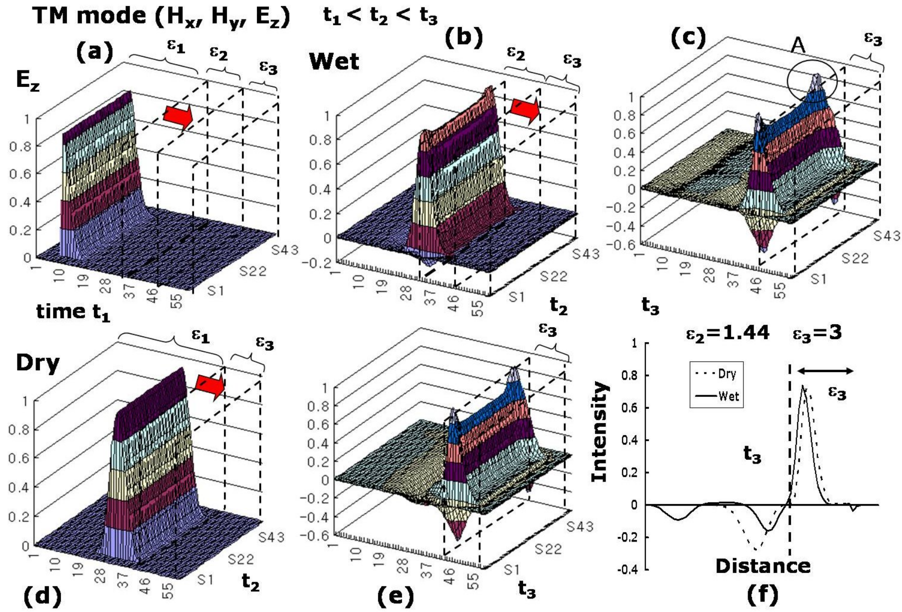

Fig. 2. Two-dimensional propagation of the electric field E_z in the TM mode (H_x, H_y, E_z) at (a) an initial time t_1, at (b) time t_2 and at (c) time t_3 in a wet system (air ($\varepsilon_1 = 1$) / water ($\varepsilon_2 = 1.446$) / resist (ε_3)) and at (d) time t_2 and (e) time t_3 ($t_1 < t_2 < t_3$) in a dry system (air ($\varepsilon_1 = 1$) / resist (ε_3)). (f) One-dimensional propagation of the electric field E_z in a wet system and in a dry system by using Eqs. (7)-(9).

III. MULT-LAYER CALCULATION

With the assumption that the thin-film stack consists of linear isotropic materials, the TE and the TM waves satisfy Maxwell equations in Eqs. (1) and (2). These equations can be derived by using transmission and reflection coefficients.

Figure 4 shows the propagation of the electric filed in three-dimensional and two-dimensional resist structures. The electric field ($\vec{E}$) is composed of TE ($\vec{E}_{TE}$)

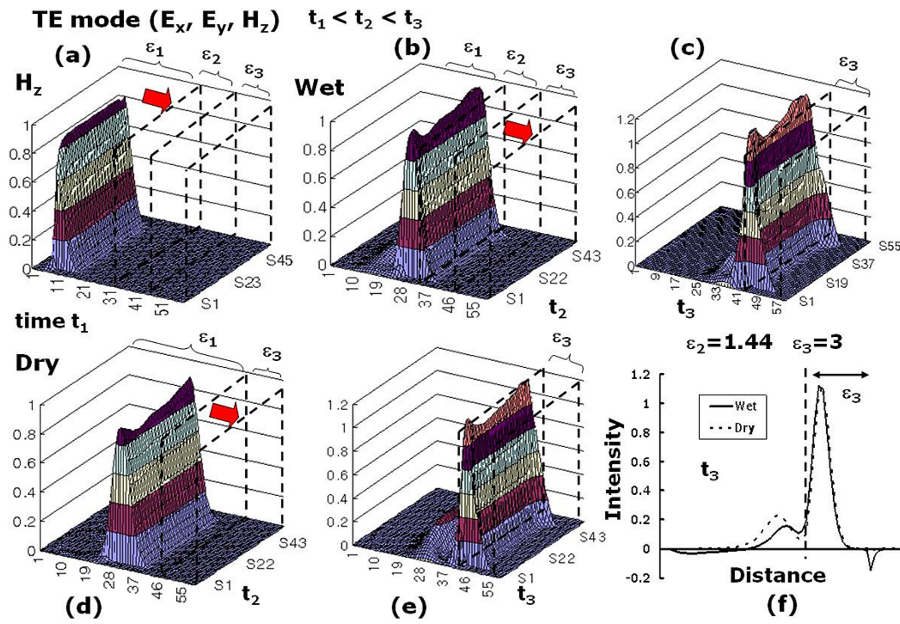

Fig. 3. Two-dimension propagation of the magnetic fields H_z in the TE mode (E_x, E_y, H_z) at (a) an initial time t_1, at (b) time t_2 and at (c) time t_3 in a wet system (air ($\varepsilon_1 = 1$) / water ($\varepsilon_2 = 1.446$) / resist (ε_3)) and at (d) time t_2 and (e) time t_3 (t_1 ¡ t_2 ¡ t_3) in a dry system (air ($\varepsilon_1 = 1$) / resist (ε_3)). (f) One-dimensional propagation of the magnetic field (H_z) in a wet system and in a dry system from Eqs. (10)-(12).

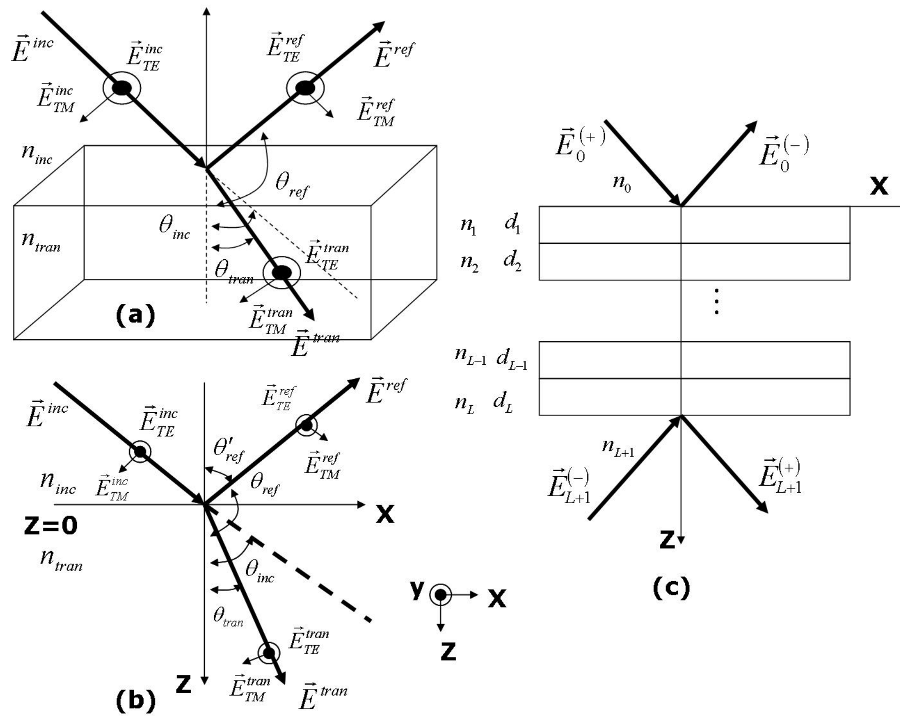

Fig. 4. Propagation structure of the electric field (a) in a three-dimensional resist, (b) in a two-dimensional resist and (c) in a two-dimensional resist according to the transfer-matrix model.

and TM ($\vec{E}_{TM}$) modes. The incident electric field ($\vec{E}^{inc}$) is reflected at the resist surface and is transmitted into the resist. The molecular structure of the resist can be assumed to be a multi-layer system with different refractive indices, so that the TE and the TM modes are distributed inside resist and react with resist molecules.

When a multi-thin-dielectric-film stack is exposed to monochromatic light, standing waves are produced in the

film. By satisfying the boundary conditions at each interface and solving Maxwell's equations, one can obtain the electric field in the thin resist film with depth z and layer j as.

$$E_j(z,\theta) = E_j \tau_{j-1,j}(\theta_j) \frac{\exp(-i\kappa z_j con\theta_j) + \rho_{j,j+1}(\theta_j)\tau_{D_j}^2(\theta_j)\exp(i\kappa_j z_j \cos\theta_j)}{1+\rho_{j-1,j}(\theta_j)\rho_{j,j+1}(\theta_j)\tau_{D_j}^2(\theta_j)} \tag{13}$$

where $\kappa_j = 2\pi n_j/\lambda$ is the propagation constant of layer j, D_j is the thickness of layer j, λ is the vacuum wavelength of the incident light and $\mathbf{n}_j = n_j - k_j$ is the complex index of refraction of layer j [5,6]. The expression for τ_{D_2} should be changed to

$$\tau_{D_2} = \exp\left(-\frac{1}{2}\int_0^{D_2}\alpha(z')\,dz'\right) \times \exp\left(-i\frac{2\pi}{\lambda}\int_0^{D_2} n_2(z')\,dz'\right), \tag{14}$$

where $\alpha = 4\pi k/\lambda$ is the absorption coefficient. In the Fresnel formulas, the transmission (τ) and the reflection (ρ) coefficients are, in TE polarization and TM polarization,

$$\rho_{ij\perp}(\theta) = \frac{\mathbf{n}_i\cos(\theta_i) - \mathbf{n}_j\cos(\theta_j)}{\mathbf{n}_i\cos(\theta_i) + \mathbf{n}_j\cos(\theta_j)}, \quad \tau_{ij\perp} = \frac{2\mathbf{n}_i\cos(\theta_i)}{\mathbf{n}_i\cos(\theta_i) + \mathbf{n}_j\cos(\theta_j)}, \tag{15}$$

$$\rho_{ij\parallel}(\theta) = \frac{\mathbf{n}_i\cos(\theta_j) - \mathbf{n}_j\cos(\theta_i)}{\mathbf{n}_i\cos(\theta_j) + \mathbf{n}_j\cos(\theta_i)}, \quad \tau_{ij\parallel} = \frac{2\mathbf{n}_i\cos(\theta_i)}{\mathbf{n}_i\cos(\theta_j) + \mathbf{n}_j\cos(\theta_i)}, \tag{16}$$

For a transfer-matrix model [7], the incident wave from a layer propagates in the $+z$ direction into layer b in Figure 4(c):

$$\begin{bmatrix} E_a^+ \\ E_a^- \end{bmatrix} = M \begin{bmatrix} E_b^+ \\ E_b^- \end{bmatrix}, \quad M = D_{0,1}P_1 D_{1,2} P_2 \ldots D_{n-1,n} P_n D_{n,b}, \tag{17}$$

where the transmission matrix $D_{m,n}$ and the propagation matrix P_m in the m-th layer are, respectively,

$$D_{m,n} = \frac{1}{t_{m,n}}\begin{bmatrix} 1 & r_{n,m} \\ r_{n,m} & 1 \end{bmatrix}, \quad P_m = \begin{bmatrix} \exp(-ik_{mz}^+ d_m) & 0 \\ 0 & \exp(ik_{2m}^+ d_m) \end{bmatrix}. \tag{18}$$

For TE and TM polarizations, the transmittance coefficient (t) and reflection coefficient (r) are, respectively,

$$r_{1,2}^{TE} = \frac{E_1^-}{E_1^+} = \frac{k_{1z}^+ - k_{2z}^+}{k_{1z}^+ + k_{2z}^+} = \frac{n_1\cos\theta_1 - n_2\cos\theta_2}{n_1\cos\theta_1 + n_2\cos\theta_2}, \quad t_{1,2}^{TE} = \frac{E_2^+}{E_1^+} = \frac{2k_{1z}^+}{k_{1z}^+ + k_{2z}^+} = \frac{2n_1\cos\theta_1}{n_1\cos\theta_1 + n_2\cos\theta_2}, \tag{19}$$

$$r_{1,2}^{TM} = \frac{H_1^-}{H_1^+} = \frac{(k_{1z}^+/\varepsilon_1) - (k_{2z}^+/\varepsilon_2)}{(k_{1z}^+/\varepsilon_1) + (k_{2z}^+/\varepsilon_2)} = \frac{(\cos\theta_1/n_1) - (\cos\theta_2/n_2)}{(\cos\theta_1/n_1) + (\cos\theta_2/n_2)},$$
$$t_{1,2}^{TM} = \frac{H_2^+}{H_1^+} = \frac{2(k_{1z}^+/\varepsilon_1)}{(k_{1z}^+/\varepsilon_1) + (k_{2z}^+/\varepsilon_2)} = \frac{2(\cos\theta_1/n_1)}{(\cos\theta_1/n_1) + (\cos\theta_2/n_2)}, \tag{20}$$

where $k_{iz}^+ = -k_{1z}^+$, $k_{2z}^- = -k_{2z}^+$ and $k_{iz}^+ = (2\pi/\lambda)\, n_i\cos\theta_i$. The superscript "+" is the downward direction and "-" is the upward direction in Figure 4(c).

IV. ANALYSIS

Figure 5 shows the TE and the TM modes inside the resist due to the incident angle, which were obtained by using a multi-layer model and a transfer-matrix model. Simulation conditions are 1.44 for the refractive index of water, 1.72 for the refractive index of resist, Dill parameters of A = 0.0014, B = 1.155 and C = 0.0364, a 120-nm resist thickness, a 86-nm ARC thickness, refractive index of n = 171 and k = –0.43 for the anti-reflective coating (ARC) and a refractive index of n = 0.883143 and k = –2.779 for the wafer. For the multi-layer system (water / resist / ARC / wafer), the electric field inside the resist can be calculated by using Eq. (13) with j = 2. For comparison with the results of a multi-layer model, the transmittance and the reflection coefficients of the TM mode in Eq. (16) are used instead of Eq. (20). When the incident TE wave and the incident TM wave are 1, respectively, the TE and TM waves change a little at incident angles below 20° both the multi-layer model in Figures 5(a) and (c) and the transfer-metric model in Figures 5(b) and (d). In both models, the TE and TM waves of the wet system are larger than those of the dry system.

Figure 6 shows the expected 45-nm critical dimensions (CDs) of 45-nm 1 : 3 line and spaces (L / S) formed in TE and TM modes with incident angles of 0°, 10° and 20° by using a multi-layer model and a transfer-metric

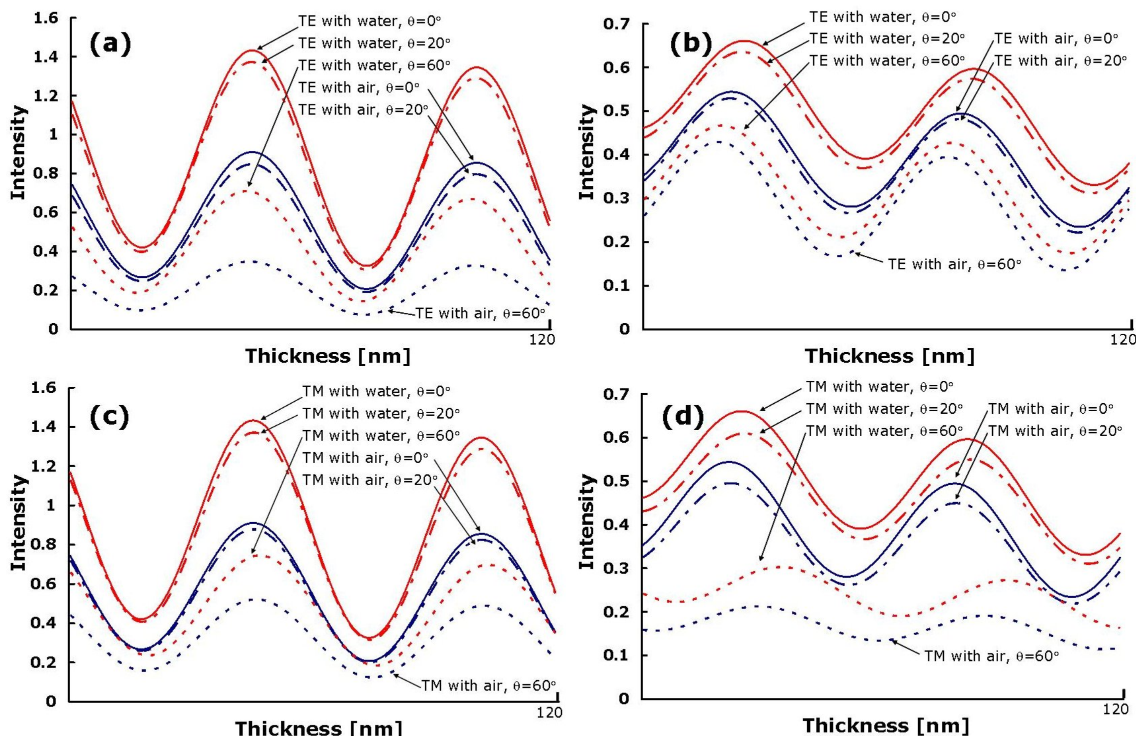

Fig. 5. Aerial images inside a resist of (a) the TE and (c) the TM modes obtained by using a multi-layer model and (b) the TE and (d) the TM modes obtained by using a transfer-matrix model at incident angles 0°, 20° and 60° in a dry system and in a wet system.

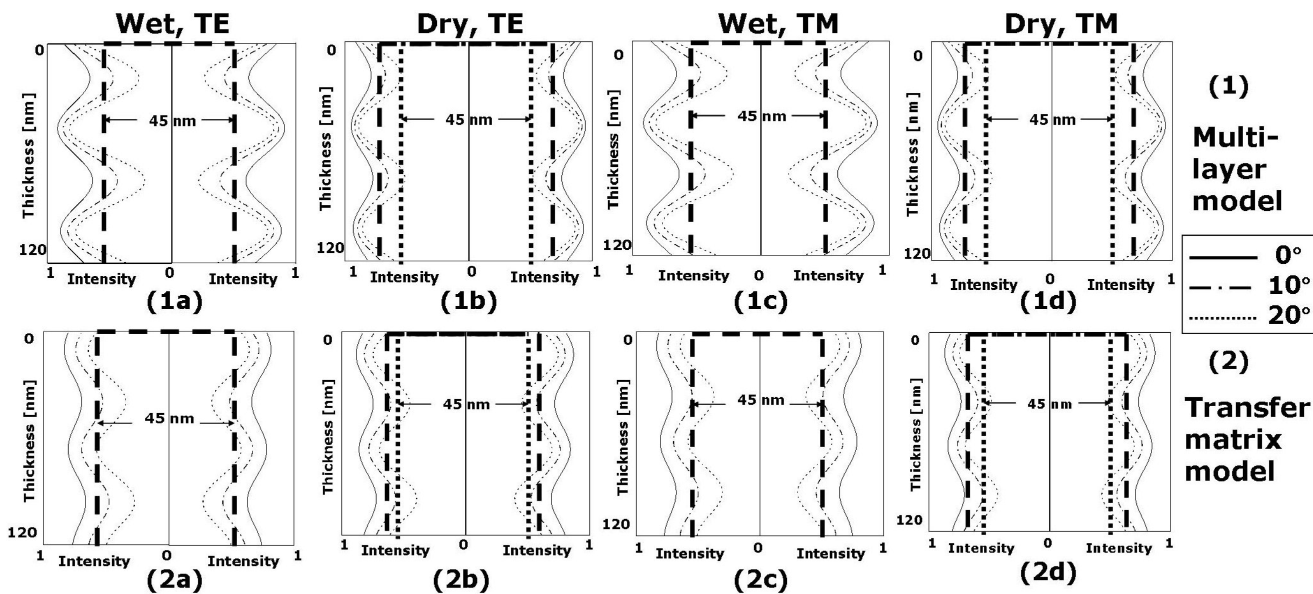

Fig. 6. Simulated 45-nm CD of 45-nm with a 1 : 3 L / S in (1a) and (2a) the TE mode in a wet system, in (1b) and (2b) the TE mode with a dry system, in (1c) and (2c) the TM with a wet system and in (1d) and (2d) TM with a dry system at incident angles 0°, 10° and 20° by using a (1) multi-layer model or a (2) transfer-matrix model.

model. Illumination conditions were a 50-nm L / S binary mask, dipole illumination with 0.825-μm offset and 0.125-μm radius, a 0.8 NA and a 1.44 refractive index of water immersion. In both TE and TM waves, the CDs of the wet system in Figures 6(1a), (1c), (2a) and (2c) are smaller than those of the dry system in Figures 6(1b), (2b), (1d) and (2d). According to the simulated results in Figure 6, the results for a multi-layer model

are similar to those for a transfer-matrix model and in each of system, the TM and TE waves are not different at incident angles below 20°.

V. CONCLUSION

For one-layer resist, the TE and TM wave propagations into a resist are described in one-dimension and two-dimensions by using the finite-difference-time-domain method. In comparison with a dry system, reflection in a wet system is smaller at the resist surface, so the wet system is expected to have reflective impact to form the fine pattern and its transmittance is expected to be larger. For a multi-layer resist, the TE and TM waves of the wet system are larger than those of the dry system and the TE and TM waves change a little at incident angles below 20° in both the multi-layer model and the transfer-metric model. However, for the 45-nm target critical dimension, the TE and TM patterns of are similar at incident angles below 20° in the wet system and the dry system.

ACKNOWLEDGMENTS

This work was fully supported by the Research fund of HYU (HYU-2008-T).

REFERENCES

[1] T. Sato, A. Endo, A. Mimotogi, S. Mimotogi, K. Sato and S. Tanaka, J. Microlith. Mricrofab. Microsyst. **5**, 043001 (2006).
[2] S.-K. Kim J. Korean Phys. Soc. **50**, 1952 (2007).
[3] S.-K. Kim and H.-K. Oh, J. Korean Phys. Soc. **51**, 1413 (2007).
[4] S.-K. Kim and H.-K. Oh, J. Korean Phys. Soc. **53**, 3578 (2008).
[5] R. Gordon and C. A. Mack, Proc. SPIE **3334**, 176 (1998).
[6] S.-K. Kim, Optical Rev. **10**, 335 (2003).
[7] S.-K. Yu, B. J. Lin, A. Yen, C.-M. Ke, J. Huang, B.-C. Ho, C.-K. Chen, T.-S. Gau, H.-C. Hsleh and Y.-C. Ku, J. Microlith. Mricrofab. Microsyst. **4**, 043003 (2005).